Nanoscale Lipophilic Prodrugs of Dexamethasone with Enhanced Pharmacokinetics

Mathilde Lorscheider, Nicolas Tsapis, Rosana Simón-Vázquez, Nicolas Guiblin, Noureddine Ghermani, Franceline Reynaud, Romain Canioni, Sonia Abreu, Pierre Chaminade, Elias Fattal

NANOSCALE LIPOPHILIC PRODRUGS OF DEXAMETHASONE WITH ENHANCED PHARMACOKINETICS

Mathilde Lorscheider[1], Nicolas Tsapis[1], Rosana Simon-Vaquez[2], Nicolas Guiblin[3], Noureddine Ghermani[1], Franceline Reynaud[1,4], Romain Canioni[1], Sonia Abreu[5], Pierre Chaminade[5], Elias Fattal[1]

[1] Institut Galien Paris-Sud, CNRS, Univ. Paris-Sud, Univ. Paris-Saclay, 92290 Châtenay-Malabry, France
[2] Immunology, Biomedical Research Center (CINBIO) and Institute of Biomedical Research of Orense, Pontevedra and Vigo (IBI), University of Vigo, Campus Lagoas Marcosende, Pontevedra, 36310, Spain
[3] École Centrale Paris, Laboratoire Structures, Propriétés et Modélisation des Solides (SPMS) UMR CNRS 8580, CentraleSupélec, Univ. Paris Saclay, 3 Rue Joliot Curie, 91190 Gif-sur-Yvette, France.
[4] School of Pharmacy, Federal University of Rio de Janeiro, 21944-59 Rio de Janeiro, Brazil.
[5] Lip(Sys)² EA7357 Lipides, systèmes analytiques et biologiques, Univ. Paris-Sud, Univ. Paris-Saclay, 92290 Châtenay-Malabry, France

Abstract

The encapsulation of glucocorticoids such as dexamethasone in nanoparticles faces two main issues: a low drug loading and the destabilization of the nanoparticle suspension due to drug crystallization. Here, we successfully formulated a prodrug of dexamethasone, dexamethasone palmitate (DXP), into nanoparticles stabilized by the sole presence of DSPE-PEG_{2000}. Two formulation processes, nanoprecipitation, and emulsion-evaporation allowed the formation of stable nanoparticles. By adjusting the drug/lipid ratio and the DXP concentration nanoparticles of DXP (DXP-NPs) with a size comprised between 130 and 300nm can be obtained. Owing to the presence of DSPE-PEG_{2000}, a high drug entrapment efficiency of 98%w/w was reached for both processes, corresponding to a very high equivalent dexamethasone drug loading around 50%w/w with the absence of crystallization upon storage at 4°C. The anti-inflammatory activity of DXP-NPs was preserved when incubated with macrophages activated with lipopolysaccharide. Pharmacokinetics parameters were evaluated after intravenous (IV) injection of DXP-NPs to healthy mice. The release of DXM from DXP-NPs in plasma was clearly controlled up to 18 hours compared to the free drug which was rapidly eliminated from plasma after administration. In conclusion, a novel type of nanoparticle combining the advantages of prodrugs and nanoparticles was designed, easy to produce with a high loading efficiency and leading to modified pharmacokinetics and tissue distribution after IV administration.

Keywords: Prodrug; Nanoparticle; Drug loading; Pharmacokinetics; Biodistribution

Table of Content Graphic

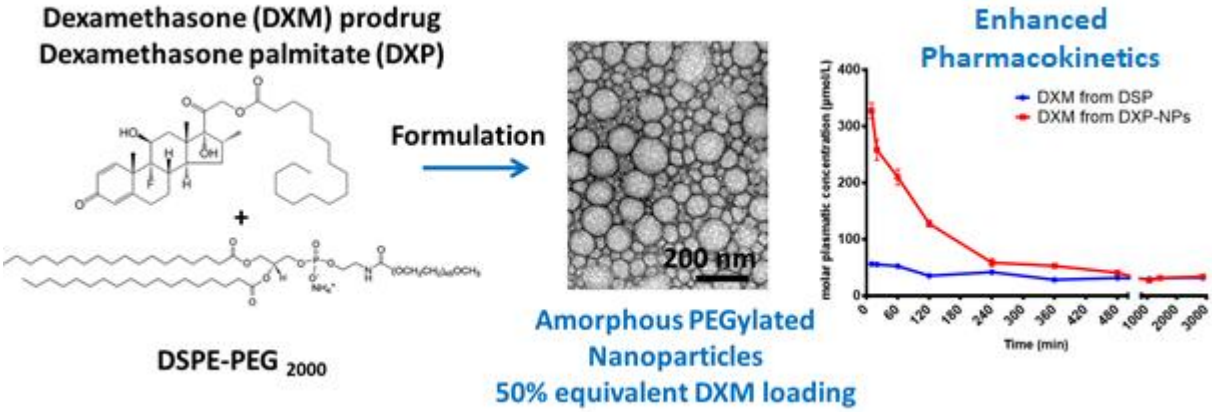

1 INTRODUCTION

Glucocorticoids (GCs) have a long history as anti-inflammatory and immunosuppressive drugs but their use is limited due to their side effects which become critical during long term therapy.[1,2] To improve GCs pharmacokinetics and increase their concentrations in inflamed therapeutic sites, the use of PEGylated nanocarriers has been considered because of their prolonged circulation in the blood stream[3] and their passive diffusion through highly permeable vasculature of inflamed tissues. [4] However, in the case of GCs and many other drugs, nanocarriers suffer from several drawbacks such as the low drug loading, the difficulty to entrap hydrophobic drugs[5,6] and the premature burst release[5,7,8] that severely hinders their clinical translation. Indeed, most physically entrapped active molecules present a drug loading comprised between 0.1 and 10%.[9] This low proportion of active drug per nanocarrier directly leads to the administration of high quantities of potentially harmful excipients such as surfactants, stabilizers (poloxamers, poly(vinyl alcohol), tween 80…), lipids or polymers. Stability of the nanosuspension may also be an issue for hydrophobic drugs. Indeed, over time, the entrapped drug is susceptible to be released in the media and crystallization is often observed due to Ostwald ripening.[5,6,10,11] In addition, the physical entrapment is often associated with a premature drug release once the formulation is injected intravenously[12]. Tsotas *et al.* demonstrated the influence of lipid composition of liposomes on dexamethasone (DXM) entrapment efficiency but never reached above 0.5 DXM/lipid molar ratio.[13] Entrapment of dexamethasone or dexamethasone acetate into poly(lactide-co-glycolide) nanoparticles led to a low drug loading of 0.2 and 0.6% w/w respectively.[5,6] In addition, drug crystallization was observed inducing the destabilization of the nanosuspension and the burst release was very important.[5,6] More recent approaches to overcome the low loading efficiency issue consisted in encapsulating within colloidal nanocarriers lipophilic prodrugs from GCs such as palmitate derivatives.[14–18] For instance, prednisolone palmitate or dexamethasone palmitate have been incorporated into liposomes with a high entrapment efficiency.[16,19] The presence of strong hydrophobic interactions between the alkyl chain of the prodrug and those of lipids forming liposomes membrane can explain the stable retention of the prodrug in the nanocarrier.[20] A lipid nanoemulsion containing dexamethasone palmitate (DXP), Limethason® or Lipotalon®, is currently on the market in Japan and Germany, indicated for rheumatoid arthritis and osteoarthritis via intra-articular injection.[21,22] Although being a crucial parameter, the burst release issue was not approached here. Therefore, to improve drug loading and limit burst release, nanocarriers consisting in solely prodrugs have been proposed.[23–26]

In the present report, a novel approach was used to formulate DXP directly into nanoparticles using a biocompatible and biodegradable lipid, Distearoyl-sn-Glycero-3-Phosphoethanolamine-N-[methoxy (polyethylene glycol)-2000)] (DSPE-PEG_{2000}) as crystallization inhibitor and colloidal stabilizer.

Nanoprecipitation and emulsion-evaporation processes were tested and compared in terms of nanoparticle size, polydispersity index, surface charge, stability, DSPE-$PEG_{2000,}$ and DXP entrapment efficiency and internal morphology. The optimal formulation obtained thanks to the emulsion-evaporation process with DXP/DSPE-PEG_{2000} concentrations of 5/2.5mg/mL was characterized for *in vitro* cytotoxicity and anti-inflammatory efficiency on activated macrophages. *In vivo* studies on mice were conducted to determine the pharmacokinetics and biodistribution showing enhanced pharmacokinetics and modified tissue distribution of the nanoparticle due to the dysopsonization effect of PEG.

2 MATERIALS AND METHODS

2.1 Materials

Dexamethasone palmitate (DXP) was purchased from Interchim (France). DSPE-PEG_{2000} (1,2-Distearoyl-sn-Glycero-3-Phosphoethanolamine-N-(methoxy(polyethylene glycol)-2000) (ammonium salt)) was obtained from Avanti Polar Lipids, Inc. (USA). Dexamethasone base (DXM) and dexamethasone acetate (DXA) were provided from Chemos GmbH (Germany). Testosterone decanoate (TesD) was obtained from Interchim (France). Dexamethasone disodium phosphate (DSP) was purchased from Fagron (The Netherlands). MilliQ water was purified using a RIOS system from Merck-Millipore (France). Chloroform HPLC-grade was obtained from Carlo Erba Reagents (France), methanol and acetonitrile HPLC-grade were purchased from VWR Chemicals (France). All experiments were performed in amber vials due to the photosensitivity of dexamethasone palmitate and DSPE-PEG_{2000}

2.2 Nanoparticle preparation

Nanoparticles were formulated either by an emulsion-evaporation or a nanoprecipitation process to obtain seven targeted final concentrations of dexamethasone palmitate with the following DXP/DSPE-PEG_{2000} ratios: 1.25/0.625; 2.5/1.25; 5/2.5; 5/5; 5/7.5; 7.5/2.5; 10/5 in mg/mL

For emulsion-evaporation, 10mL of milliQ water was prechilled at 4°C. The desired amounts of DXP (12.5; 25; 50; 75 or 100mg) and DSPE-PEG_{2000} (6.25; 12.5; 25; 50 or 75mg) were dissolved in 1mL chloroform. The organic phase was then injected into the water phase thanks to a solvent-compatible syringe (Injekt®, B.Braun) and a 20Gx$2^{3/4}$ needle. The mixture was then pre-emulsified by vortexing for 30 seconds before being placed under ultrasonication during 2min at an amplitude of 40% in an ice bath. The organic phase evaporation was performed under reduced pressure using a rotary evaporator (Büchi). After full evaporation of the solvent, the suspension volume was completed to 10 mL with Milli-Q water in a volumetric flask and nanoparticles were stored at 4°C protected from light.

For nanoprecipitation, DSPE-PEG_{2000} (6.25; 12.5; 25; 50 or 75mg) was dissolved in 5mL milliQ water at 60°C. DXP (12.5; 25; 50; 75 or 100mg) was dissolved in 1mL acetone and then slowly injected into the aqueous phase under magnetic stirring. After 5min stirring, the preparation was evaporated under reduced pressure using a rotary evaporator. After full evaporation of the solvent, the suspension volume was completed to 10mL with Milli-Q water in a volumetric flask and nanoparticles were stored at 4°C protected from light. Osmolality was measured on a freezing point depression automatic micro osmometer (Type 13/13DR autocal, Roebling, Germany).

2.3 Size and zeta potential measurement

Size and zeta potential were determined with a Zetasizer Nano-ZS from Malvern Instrument (UK), based on quasi-elastic light scattering. The measurement was performed in triplicate at an angle of 173° at 25°C. Hydrodynamic diameter (d_H), polydispersity index (PdI) and zeta potential were recorded on 1/10 diluted samples in milliQ water for size measurements or in NaCl 1mM for zeta potential measurements.

2.4 Transmission electron microscopy (TEM)

Transmission electron microscopy was performed at I2BC (CNRS, Gif-sur-Yvette, France). A volume of 5µL of the nanoparticle suspension at 5mg/mL DXP was deposited for 1 minute on 400 mesh formwar-coated copper grids. Negative staining was performed by addition of a drop of uranyl acetate at 2% w/w for 30 seconds. Excess solution was removed and grids were left to dry before observation. The observations were carried out on a JEOL JEM-1400 microscope at an acceleration voltage of 80KV. Images were acquired using an Orius camera (Gatan Inc, USA).

2.5 X-ray powder diffraction

X-ray powder diffraction (XRPD) measurements were performed using a Rigaku rotating copper anode automated diffractometer operating at 50kV and 200mA using Cu Kα radiation. Nanoparticles suspensions were concentrated with Amicon 100kDa, the concentrate was gently introduced into quartz capillaries before sealing them. The intensity of the diffracted X-ray beam was measured as a function of the theta angle (1 to 60°).

2.6 Entrapment efficiency

After DXP nanoparticles (DXP-NPs) preparation, quantification of encapsulated DXP and DSPE-PEG_{2000} was performed with HPLC coupled to an evaporative light-scattering detector (ELSD, Eurosep, Cergy, France) and a UV detector (785A, Applied Biosystems). DXP was detected with both detectors and DSPE-PEG_{2000} was only detected with ELSD detector. UV detection was performed at 240nm wavelength and ELSD detection settings were a nebulization temperature of 35°C and an evaporation

temperature of 45°C. An autosampler (Series 200, Perkin Elmer) was employed connected to a Perkin Elmer pump and both detectors UV and ELSD. The SymmetryShieldTM RP18 column (5 µm, 250×4.6 mm; Waters, France) was maintained at room temperature, the mobile phase was composed of MeOH:ACN:Ammonium acetate (pH 4.00, 200mM) 70:20:10 added with 0.043% acetic acid and 0.104% trimethylamine, flow rate was set at 1mL/min.

To separate DXP-NPs form non-encapsulated molecules, ultracentrifugation was performed at 40000rpm (=109760g) during 4h at 4°C (Beckman Coulter Optima LE-80K ultracentrifuge, 70-1Ti rotor). The supernatant was delicately removed to avoid resuspension of the pellet and freeze-dried for 24h (Alpha 1-2 LD Plus, Bioblock, France) after freezing in liquid nitrogen (-196°C). Lyophilisates were dissolved in methanol to reach suitable concentrations within the range of the calibration curve. A volume of 30µL of samples dissolved in MeOH was injected and analyzed during 12min. Retention times were 7min and 9min for DXP and DSPE-$PEG_{2000,}$ respectively. The concentration ranges of the calibration curves were 12.5-750µg/mL for DXP and 37.5-375µg/mL for DSPE-PEG_{2000}. ELSD detection calibration curves followed a power law model, equations and correlation coefficients were $y=219.71x^{1.2458}$, $R^2=0.9959$ for DXP and $y=144.12x^{1.2714}$, $R^2=0.9991$ for DSPE-PEG_{2000}, respectively. UV calibration curve of DXP followed a linear model, $y=486.2x+4.6095$, $R^2=0.9987$. Entrapment efficiency was calculated as the DXP or DSPE-PEG_{2000} amount encapsulated compared to the initial amount weighted for the DXP-NPs preparation. Drug loading results correspond to the proportion equivalent DXM amount encapsulated compared to the total mass of the DXP-NPs.

2.7 Surface PEG density

PEG density at the surface of DXP-NPs 5mg/mL prepared through nanoprecipitation or emulsion-evaporation was quantified using data presented thereafter. DXP-NPs density was calculated as an average between ratios of $\rho_{DXP}=1.12g/cm^3$ and $\rho_{DSPE\text{-}PEG2000}=1g/cm^3$ according to the entrapment efficiency of each component, the average diameter of the nanoparticles, the molar mass of DSPE-PEG_{2000} is $M_{DSPE\text{-}PEG}=2805.54g/mol$. Masses of DXP and DSPE-PEG_{2000} in NPs were respectively 50mg and 25mg with the respective percentages of encapsulated DXP and DSPE-PEG_{2000} depending on the technique used.

Using these data, the surface area (S_{sp}, specific surface) of the suspension depends on ρ (nanoparticle density) and d_H (nanoparticle average diameter) and can be calculated as (Equation 1).

Equation 1 $$S_{sp} = \frac{6}{\rho d_H}$$

Thus, the available surface ($S_{available}$) in a suspension can be calculated using Equation 2.

Equation 2 $S_{available} = S_{sp} \times (m_{DXP} + m_{DSPE-PEG})$ where m_{DXP} and $m_{DSPE\text{-}PEG}$ are the actual masses of DXP and DSPE-PEG_{2000} found in a formulation.

The number of DSPE-PEG_{2000} in the suspension can be calculated using Equation 3

Equation 3 $N_{DSPE\text{-}PEG} = \frac{m_{DSPE-PEG}}{M_{DSPE-PEG}} \times N_A$ where N_A is the Avogadro number

Using these three values, it is possible to deduce the surface available per PEG chain on the surface of the nanoparticles (Equation 4).

Equation 4 $Surface_{PEG} = \frac{S_{available}}{N_{DSPE-PEG}}$

The PEG density is expressed as surface area (nm^2) per PEG chain.

2.8 Cell culture

The murine macrophage cell line RAW 264.7 obtained from ATCC (USA) was cultured in 75 cm^2 flask with 15 mL of DMEM supplemented with 10% FBS, 10 000 unit/mL of penicillin and 10 mg/mL of streptomycin, in a humidified incubator at 37°C supplied with 5% CO_2. Cells were split twice per week at 1/10 ratio using a scraper to detach them and were used between passages 3 to 20 after thawing.

2.9 Cell viability

The influence of the DXP-NPs on cell viability was assessed using the MTT (3-[4,5-dimethylthiazol-2-yl]-3,5-diphenyl tetrazolium bromide) colorimetric assay [27] that evaluates mitochondrial activity. Cells were seeded in 96-well plates (TTP, Zurich, Switzerland) at a density of $8x10^3$ cells/well in 100 µL of culture medium, and were left overnight in the incubator. DXP-NPs were diluted in culture medium at various concentrations (37.5-450µg/mL DXP), 100µL of theses dilution were added on cells, the culture medium was used as a negative control. DXP-NPs alone in the culture medium, without cells, were also tested to check their potential interference with the MTT assay. Plates were incubated for 24 hours and the yellow tetrazolium MTT (3-(4, 5-dimethylthiazolyl-2)-2,5-diphenyltetrazolium bromide) was added at a final concentration of 500 µg/mL and incubated for another hour. The MTT is reduced by metabolically active cells to form the purple formazan crystals. After the formation of the crystals, the medium was discarded and replaced by 200 µL of dimethyl sulfoxide (DMSO) to dissolve crystals and the absorbance was measured at 570nm. The formula used to calculate cell viability was the following: (Abs: absorbance)

$$\%\ \text{cell viability} = \frac{(\text{Abs cells+NPs}) - \text{Abs(NPs+DMEM)}}{\text{Abs cells} - \text{Abs DMEM}} \times 100$$

Following the same protocol, dexamethasone sodium phosphate (DSP) was tested as a positive control. Serial dilutions in culture medium were performed ranging from 41 to 657µg/mL DSP. To compare DXP-NPs and DSP, tested concentrations were calculated as dexamethasone base equivalents (*eq.DXM*), corresponding to the active drug. All measurements were performed in triplicate.

2.10 Cytokine quantification

For the cytokine quantification, RAW 264.7 cells were seeded in 24-well plates at a cell density of $4x10^4$ cells/well in culture medium and were incubated for 48 hours until 80% confluency. Then, the medium was replaced by fresh medium alone or fresh medium with LPS at 0.1 µg/mL to induce inflammation, and plates were incubated another 3 hours. Afterwards, nanoparticles produced by emulsion-evaporation (5/2.5 mg/mL DXP/DSPE-PEG_{2000}) at three concentrations diluted in culture medium: 1, 10 and 100µg/mL of DXP and free dexamethasone phosphate (DSP) at 82µg/mL in culture medium, which correspond to 100µg/mL DXP considering molecular weight ratio, were added. Culture medium alone was used as negative control and LPS 0.1 µg/mL as a positive control. After 24 hours of incubation with the treatments, cell supernatants were collected and frozen at -20°C until analysis was performed. Cells were detached and counted. Mouse inflammatory cytokines TNFα, MCP-1, IL-10, and IL-6 were quantified using a Cytometric Beads Array (CBA) detection kit (BD Biosciences, USA). In each test tube, 50µL of mouse inflammation capture bead suspension was added, completed with either 50µL of standards solution (20-5000pg/mL) or 50µL of supernatants samples. Phycoerythrin (PE) detection reagent was added 50µl to each tube and incubation during 2h at room temperature was performed. Samples were washed with 1mL wash buffer provided in the kit and tubes were centrifuged (200g, 5min) to recover the pellet. 300µL of wash buffer was added to resuspend the pellet and samples were quantified with the BD Accuri C6 Cytometer (BD Biosciences, USA). Cytokines results were analyzed with the FACP Array™ Software and were obtained as pg/mL concentrations. All measurements were performed in triplicate. Statistical analysis was performed with two-way ANOVA followed by Tukey's post-test using GraphPad Prism.

2.11 *In vivo* studies

In vivo experimental procedures using DBA/1OlaHsd mice were approved by the ethical committee No 026 and by the French ministry of education and research (Accepted protocol No 2842-2015110914248481_v5). The number of animals was determined according to the power analysis method [28]. 9-12-week-old male DBA/1OlaHsd mice were purchased from Envigo (UK) and let for one week after shipping for adaptation before starting experiments. Mice were kept in a separate animal room under climate-controlled conditions with a 12h light/dark cycle, housed in polystyrene cages containing wood shavings and fed standard rodent chow and water *ad libitum*. Mouse colonies were screened and determined to be pathogen-free.

2.12 Pharmacokinetics and biodistribution

Nanoparticles prepared by emulsion-evaporation 5/2.5 mg/mL (DXP/DSPE-PEG_{2000}) as described above were half-diluted in PBS to obtain a final concentration of 2.5mg/mL DXP, which corresponds

to an equivalent of 1.55mg/mL DXM. A control of dexamethasone disodium phosphate (DSP) in PBS was prepared to obtain a final concentration of 1.55mg/mL (*eq. DXM)*. DBA/1OlaHsd male mice aged 10-12 weeks were divided into two groups. One group was administered with the nanoparticle suspension and the other received the control. The administration was performed by IV injection in the tail vein at 12mg/kg (*eq. DXM*), an intermediate dose in the range found in the literature for efficacy in mice (1-60mg/kg)[25,29]. For each group, 10 pharmacokinetics time points were selected with 7 mice per time point. Blood sampling was achieved by terminal cardiac puncture using a 25G needle while mice were previously deeply anesthetized with a lethal dose of pentobarbital. Immediately after sampling, blood was centrifuged to recover plasma which was stored at -80°C and extracted to quantify DXP and DXM as described after. For each time point, 5 mice out of 7 underwent organ sampling after a cardiac puncture. Liver, spleen, kidneys, and lungs were removed and stored at -80°C for further dosing. PK analysis was performed using the PK solver plugin from Excel.

2.12.1 DXP and DXM quantification in plasma

To quantify DXP and DXM in plasma, an extraction process was developed. 100µL of plasma samples were introduced into centrifugation tubes and 100µL of the internal standards (IS) mixture, testosterone decanoate (TestD) for DXP and dexamethasone acetate (DXA) for DXM, both at 4µg/mL in acetonitrile were added and vortexed for 30 seconds. 3mL of a 9/1 chloroform/methanol (v/v) mixture was added and tubes were vortexed vigorously for 3 minutes to precipitate proteins. Centrifugation was performed at 3500rpm (=1690g) for 30min (ST16R centrifuge, rotor TX-400, Thermo Scientific, France). The supernatant organic phase was recovered and evaporated using an evaporator under nitrogen gas flow (Sample concentrator, Stuart, UK). Dried samples were dissolved into 200µL acetonitrile and DXP or DXM were quantified by HPLC-UV. Each sample was analyzed twice, once with the DXP quantification method, second with the DXM quantification method.

A Waters 717 Plus autosampler chromatographic system was employed equipped with a Waters 1525 binary HPLC pump, a Waters 2487 dual λ absorbance UV detector, and a Breeze software. The analysis was performed at 240nm wavelength using a SymmetryShieldTM RP18 column (5 µm, 250×4.6 mm; Waters, Saint-Quentin-en-Yvelines, France). The column temperature was maintained at 40°C. The mobile phase was composed by a mixture of acetonitrile and milliQ water: 85/15 v/v for DXP and 35/65 v/v for DXM. The mobile phase flow rate was 1.2mL/min, the injection volume was 50µL and the run time was 30min. Retention times were 24min and 9min for DXP and DXM, respectively, 21min for TestD (IS of DXP) and 26min for DXA (IS of DXM). Calibration curves of DXP and DXM were linear, respectively in the range 0.5-100µg/mL (R^2=0.9997, y=0.2199x-0.0165,

LOQ=0.5µg/mL, LOQ=0.16µg/mL) and 0.1-100µg/mL (R^2=0.9974, y=1.056x+0.1445, LOQ=0.1µg/mL, LOQ=0.033µg/mL).

Regarding short time points (10min, 20min), DXP and DXM concentrations were above the linearity range of the calibration curve. A second calibration curve for each molecule was determined with 50µL plasma completed to 100µL with milliQ water. Following extraction steps were the same as previously described. Calibration curves "50µL plasma" of DXP and DXM were linear, respectively in the range 50-800µg/mL (R^2=0.9808, y=0.2229x-3.2128) and 20-400µg/mL (R^2=0.9986, y=0.7178x-0.059).

2.12.2 DXP and DXM quantification in organs

Organs were homogenized in PBS using a micro-pestle coupled with a turbine at 2038rpm during the time needed to obtain a liquid preparation, approximately 5min. DXM and DXP were extracted from the homogenate using the same method than plasma extraction, beginning with 100µg of homogenate for liver and kidneys, 25µg for spleen and lungs completed up to 100µg with milliQ water. 100µL of internal standard mixture TestD and DXA at 4µg/mL was added and vortexed 30sec, followed by the addition of 3mL of 9/1 chloroform/methanol (v/v), vortexed for 3min and centrifuged in the same conditions as above. The organic phase was evaporated and 200µL acetonitrile was added and mixed during 1.5min. This final sample was analyzed by HPLC-UV, using the same conditions as plasma samples.

3 RESULTS & DISCUSSION

3.1 Formulation process

Two different formulation processes were tested to produce DXP nanoparticles coated with phospholipids coupled to PEG. As DXP is highly hydrophobic and known to be prone to crystallization in aqueous suspension[30], DSPE-PEG_{2000} was added to the prodrug to limit its crystallization and to inhibit Ostwald ripening. Indeed, Ostwald ripening due to the high DXP proportion was already described for DXP microemulsions[31] and for palmitate derivatives such as ascorbyl palmitate nanocrystals. [32] DSPE-PEG_{2000} is an excipient mainly used in the formulation of clinically applied liposomes and in solid-lipid nanoparticles.[33] To choose the process best suited for further IV administration of GCs nanoparticles, several DXP/DSPE-PEG_{2000} ratios were selected with a fixed DXP initial concentration of 5mg/mL. Both processes led to the formation of nanoparticles. When applying nanoprecipitation, the hydrodynamic diameter did not vary, regardless of the DXP/DSPE-PEG_{2000} ratio with nanoparticles around 230-250nm (Figure 1a). For emulsion-evaporation, smaller nanoparticles whose diameter was in the range of 120-130nm were obtained, independently of the DXP/DSPE-PEG_{2000} ratio (Figure 1a). This difference can be explained when examining more closely

the process parameters. During nanoprecipitation, DXP was dissolved in acetone and DSPE-PEG_{2000} was solubilized in water at 60°C. Heating the aqueous phase at 60°C eases the dissolution of the PEGylated lipid and promotes the diffusion of acetone in water during the injection step to favor the fast formation of nanoparticles. On the contrary, heating the aqueous phase during emulsion-evaporation could lead to the fast evaporation of chloroform during the emulsion step with ultrasonication, resulting in the destabilization of the primary emulsion and no DXP-NPs formation. For this reason, we opted to dissolve at room temperature DSPE-PEG_{2000} with DXP in chloroform for the emulsion-evaporation process. Thereby, the presence of DXP and DSPE-PEG_{2000} together in chloroform favors their interaction and leads to the formation of smaller nanoparticles. The smaller size of emulsion-evaporation DXP-NPs may also arise from a reduced interfacial tension of the chloroform-water interface due to the presence of the PEGylated lipid.

To determine the impact of DXP concentration on nanoparticle size, four DXP concentrations were then tested 1.25, 2.5, 5 and 10mg/mL for both formulation processes with a constant 2/1 DXP/DSPE-PEG_{2000} ratio. Figure 1b clearly shows that d_H increases as DXP concentration increases using the nanoprecipitation process. Very polydisperse nanoparticles of 300nm at a DXP concentration of 10mg/mL were obtained. In the case of nanoprecipitation, nanoparticle size can be adjusted by tuning the DXP initial concentration. On the contrary, the emulsion-evaporation process led to the formation of monodisperse nanoparticles around 130nm, with a slight increase of size up to 170nm, for the highest concentration tested.

Our rationale was to design a nanoparticle suspension with high drug concentration and low concentration of excipients for IV administration, the DXP/DSPE-PEG_{2000} 5/2.5mg/mL conditions were therefore selected for remaining experiments. For both preparation methods, formulations were characterized and compared in terms of stability, entrapment efficiency, drug loading, and DSPE-PEG coating.

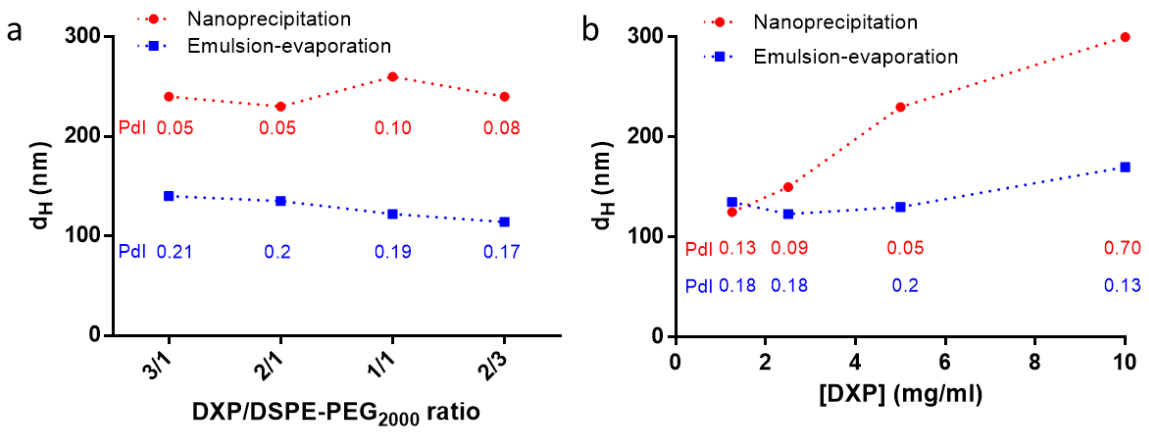

Figure 1. **a**. Impact of the DXP/DSPE-PEG_{2000} weight ratio on the size of the obtained nanoparticles (constant final DXP concentration of 5mg/mL). The ratios 3/1, 2/1, 1/1 and 2/3 were tested through nanoprecipitation (red circles) and emulsion-evaporation (blue squares) processes. **b**. Evaluation of the impact of DXP concentration in both nanoprecipitation (red circles) and emulsion-evaporation (blue squares) processes with a constant 2/1 DXP/DSPE-PEG_{2000} ratio.

3.2 Size, zeta potential and stability over time

After preparation of DXP/DSPE-PEG 5/2.5mg/mL nanoparticles by either nanoprecipitation or emulsion-evaporation, their size, polydispersity index (PdI) and zeta potential were followed during 37 days to confirm the stability of the suspension (Figure 2). Formulation storage at 4°C and room temperature were compared. Emulsion-evaporation-prepared DXP-NPs stored at 4°C were clearly more stable in terms of size, PdI and zeta potential. Under 4°C storage, nanoparticle hydrodynamic diameter (d_H) was kept around 130±3nm (Figure 2a) up to 37 days after preparation. Under the same storage conditions, the zeta potential and the PdI were stable around -50 to -60 mV and 0.2, respectively. On the contrary, at room temperature, size increased after 4 days and on day 14, a clear destabilization of the nanosuspension appeared, characterized by a size increase of 40%, associated with a rise of polydispersity and zeta potential (Figure 2a). On day 21 and later, no size and zeta potential measurements could be performed for samples stored at room temperature due to precipitation resulting from the formation of DXP crystals within the precipitate as evidenced by optical microscopy (Figure S1). By contrast, the nanoprecipitation process yielded stable nanoparticles which mean diameter remained around 230nm at 4°C and presented size increase at room temperature on day 37 due to their destabilization (figure 2b). DXP-NPs polydispersity index was kept below 0.2 highlighting a rather monodisperse population. The zeta potential was also stable ranging from -50 to -60mV. This high negative surface charge was able to promote electrostatic repulsion between nanoparticles and prevents aggregation and destabilization of the preparation.

These nanoparticles prepared by either emulsion-evaporation or nanoprecipitation techniques, with high concentrations of DXP/DSPE-PEG_{2000} 5/2.5mg/mL, present a clear advantage being long term stable at 4°C without the need of purification steps or freeze-drying. This characteristic is an important point in terms of ease of production.

3.3 Morphology and internal structure of the nanoparticles

TEM observations were consistent with dynamic light scattering measurements (Figure 3). Indeed, emulsion-evaporation process led to small spherical nanoparticles, with higher polydispersity than those obtained by nanoprecipitation. The mean diameter of the emulsion-evaporation-prepared nanoparticles was lower than 200nm. Figure 3b presents monodisperse and spherical DXP-NPs prepared by nanoprecipitation. Their hydrodynamic diameter above 200nm confirmed DLS studies.

No crystals or crystalline structure could be observed on these images. DXP-NPs suspensions were analyzed by X-ray diffraction to determine their internal structure. Using both formulation processes, the resulting DXP-NPs were analyzed the day of preparation and 3 weeks after storage at 4°C. They were compared to crystalline DXP form obtained from recrystallization in acetone that gives needle-shaped crystals[19,30]. The diffractogram of recrystallized DXP after acetone evaporation is typical of a crystalline structure with many diffraction peaks (Figure 4 bottom) as described by Doi *et al* .[30]. By contrast, almost no diffraction peaks can be observed for DXP-NPs either freshly prepared or 3 weeks old, regardless of the preparation technique (Figure 4 top). The diffractogram of DXP-NPs presents a "bump" which is typical of the presence of an unorganized amorphous system. Results clearly show that neither DXP nor DSPE-PEG_{2000} present a crystalline organization. In addition, the amorphous nanoparticles appear stable upon storage at 4°C, a clear advantage for further clinical use. Therefore whatever the process of formulation, DXP-NPs remain amorphous and stable under storage at 4°C as no crystal is observed microscopically or detected by X-ray diffraction. As demonstrated for other excipients such as Pluronic F127[34] and HPMC[35], the presence of DSPE-PEG_{2000} seems to slow down the nucleation and crystal growth of DXP in the suspension. During the formation of DXP-NPs, the DXP palmitate chain interacts with the stearate chains of DSPE-PEG_{2000} thanks to strong hydrophobic interactions introducing some disorder. This strong interaction might also be responsible for the limitation of Ostwald ripening. Moreover, the hydrophilic PEG chains exposed at nanoparticle surface improve stability by steric hindrance.

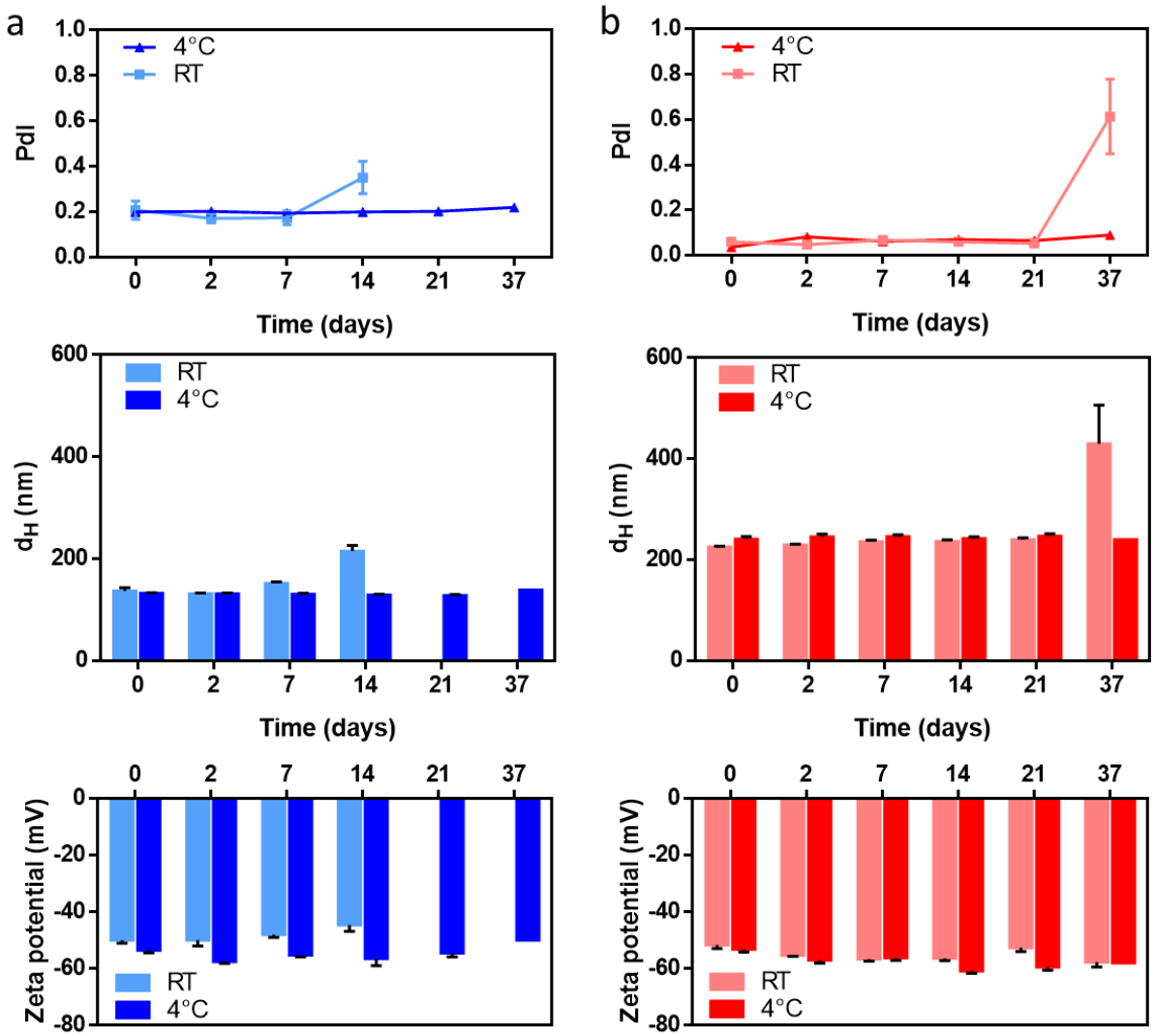

Figure 2. Size, PdI and zeta potential stability of DXP/DSPE-PEG_{2000} 5/2.5 mg/mL nanoparticles, at room temperature (RT) or 4°C. **a**. emulsion-evaporation, **b.** nanoprecipitation. Results are presented as mean±SEM (n=5 at least).

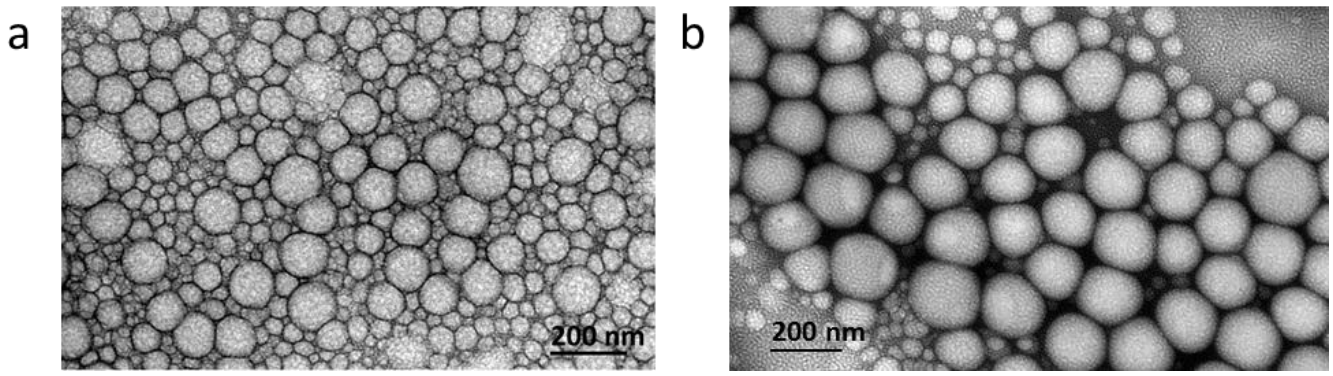

Figure 3. DXP/DSPE-PEG_{2000} 5/2.5mg/mL nanoparticles imaged by TEM after negative staining. **a**. emulsion-evaporation and **b**. nanoprecipitation process.

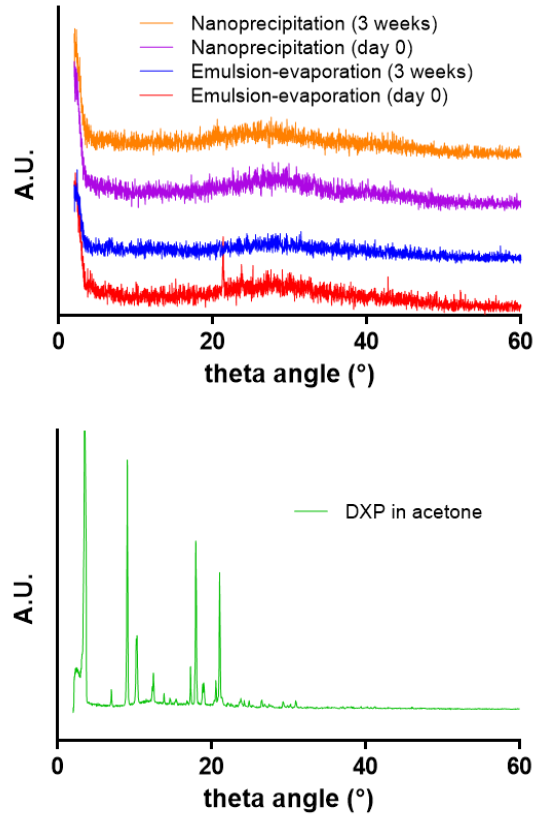

Figure 4. X-ray diffractogram of DXP-NPs obtained directly after their formulation (day 0, emulsion-evaporation (red) and nanoprecipitation (purple)), or after 3 weeks storage at 4°C (emulsion-evaporation (blue) and nanoprecipitation (orange)), and DXP crystals (green).

3.4 Entrapment efficiency and drug loading

During nanoparticles preparation, DSPE-PEG_{2000} is expected to associate strongly with DXP thanks to hydrophobic interactions between the distearoyl chains of DSPE-PEG_{2000} and the palmitate chain of DXP. Entrapment efficiency was determined by quantifying, on one hand, the amount of DSPE-PEG_{2000} associated to DXP-NPs, and on the other hand, the amount of DXP in DXP-NPs as it is related

to the potential amount of DXM that could be delivered. A simple method of HPLC-ELSD that can separate and detect both components in a single injection on the same chromatogram was developed. After separation by ultracentrifugation, non-encapsulated DXP and DSPE-PEG_{2000} in the supernatant were quantified and their amount in NPs was calculated indirectly. The proportion of encapsulated DSPE-PEG_{2000} presented variations according to the formulation process (Figure 5a). Nanoprecipitation led to 20% of encapsulated DSPE-PEG_{2000} whereas 53% was encapsulated thanks to emulsion-evaporation process ($p < 0.05$, unpaired t-test). The difference of DSPE-PEG_{2000} entrapment efficiency between the two processes, nanoprecipitation 20%w/w and emulsion-evaporation 53%w/w, could be linked to DSPE-PEG_{2000} solvent affinity (acetone or chloroform) and its impact on hydrophobic interaction between lipids and DXP occurring during nanoparticles preparation. Considering the amounts of encapsulated DXP and DSPE-PEG_{2000}, the DXP prodrug loading and the corresponding active drug DXM loading can be calculated (Figure 5b). Nanoprecipitated nanoparticles present a high DXP loading (91%w/w), corresponding to an equivalent of 56% of DXM of the DXP-NPs total mass. Emulsion-evaporation leads to 78%w/w DXP loading corresponding to an equivalent of 48%w/w DXM loading, meaning that half of the total mass of DXP-NPs is composed of the active drug. When comparing to literature, these drug loadings are very high. Indeed, the formulation of DXP in the lipid emulsion Limethason® exhibits a low drug loading of 4%w/w DXP/lipids resulting in an equivalent DXM loading of 2.5% w/w. We suspect that this low drug loading was chosen due to the possible issues of crystallization and stability of this formulation at higher DXP concentrations. Here, despite the differences of DSPE-PEG_{2000} encapsulated by both methods, 98% of the initial amount of DXP was detected in DXP-NPs with no significant differences ($p > 0.05$, unpaired t-test). Irrespective of the formulation process and thanks to the presence of palmitate chain on dexamethasone, the highest possible drug entrapment efficiency was reached.

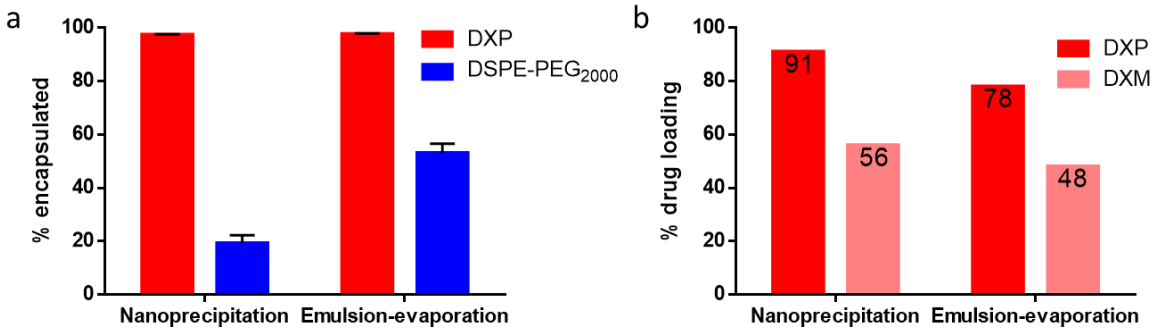

Figure 5. a. DXP (red) and DSPE-PEG (blue) entrapment efficiency in DXP-NPs prepared by nanoprecipitation or emulsion-evaporation. **b.** Corresponding DXP (red) and equivalent DXM (light red) loading for both formulation processes. Results are presented as mean±SEM (n=7).

Because nanoparticle formulation process clearly impacts on the PEGylated lipid number in nanoparticles, we have calculated the area occupied by each PEG chain on nanoparticle surface in order to evaluate PEG density. To calculate this density, we need to hypothesize that 100% of PEG chains are situated on the surface of the nanoparticles and not in the matrix/core. Since PEG is hydrophilic and DSPE hydrophobic, it seems realistic that most of it stand at the surface of nanoparticles, with the DSPE moiety inserted in the matrix while the PEG chain is exposed in contact with water.

For emulsion-evaporation, data used for PEG density calculation are ρ=1.09g/cm^3, the average diameter of the nanoparticles is d=130nm and the percentages of encapsulated DXP=98% and encapsulated DSPE-PEG$_{2000}$=53% for a DXP/DSPE-PEG$_{2000}$ 5/2.5 mg/mL suspension. Using these data, the surface available per PEG chain on the surface of the nanoparticles formed by emulsion-evaporation is therefore 0.93nm^2/PEG. For nanoprecipitation process, after injecting correct values: ρ=1.11g/cm^3, d=230nm, one finds that the available surface per PEG chain is 1.18nm²/PEG. The emulsion-evaporation process was therefore considered as gold standard formulation method with small and stable nanoparticles, high drug loading and high PEG density, favorable to good opsonin repulsion. Indeed, to allow passive diffusion through high permeable vessels, nanoparticle size range of 50-400nm is preferred with better accumulation when size is below 200nm.[36–39] Regardless of the formulation technique, DXP-NPs presented suitable characteristics for this type of indication. However, nanoparticles obtained by the emulsion-evaporation process, using a DXP concentration of 5mg/mL, led to smaller and monodisperse nanoparticles that could be used in the treatment of inflammation diseases. Moreover, for IV administration, a nanoparticle suspension with a high concentration of active substance will be preferably chosen in order to inject a volume as small as possible. NP characterization suggests that DXP-NPs prepared by emulsion-evaporation method are optimally producing small and stable nanoparticles with high drug loading and high PEG density.

3.4.1 Cytotoxicity and anti-inflammatory activity

A range of DXP-NPs concentrations from 37.5µg/mL up to 450µg/mL (corresponding to 23.3-280µg/mL *eq.DXM)* was tested and compared to the water-soluble free drug, dexamethasone sodium phosphate (DSP) on macrophages. According to ISO guideline for MTT assay, potential cytotoxicity is defined when cell viability decreases below 70% of the control.[40] Figure 6 clearly shows DXP-NPs presented no cytotoxicity up to DXM equivalent concentration of 280µg/mL, whereas no decrease in cell viability was observed for DSP in the concentration range tested. In addition, 280µg/mL (eq.DXM) is a rather high concentration that is unlikely to be reached during *in vivo* studies after IV injection.

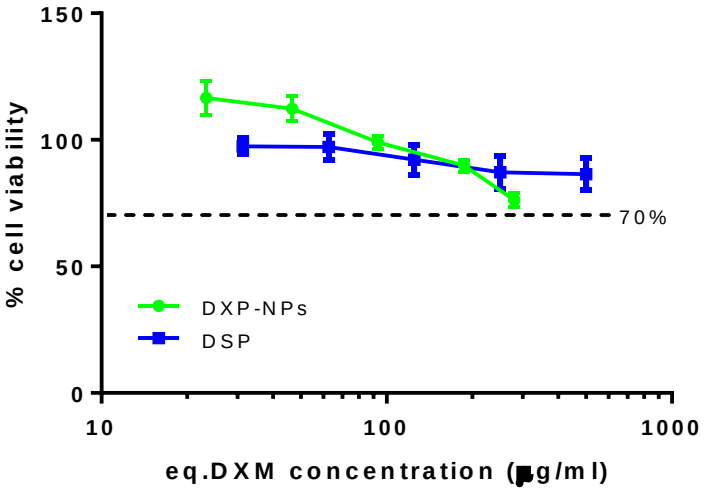

Figure 6. Raw 264.7 macrophages viability after 24h exposure to DXP-NPs prepared by emulsion-evaporation (green circles) or DSP solution (blue squares) at different concentrations. Concentrations are expressed as equivalent DXM. Results are presented as mean±SEM (n=3).

To ensure that the anti-inflammatory activity of DXM was preserved after formulation, the release of pro-inflammatory cytokines (MCP-1, IL-10, IL-6, TNFα) by LPS-activated Raw 264.7 macrophages into the cell culture medium was quantified after their exposure to DXP-NPs at different concentrations (1; 10; 100µg/mL DXP) or free DSP at 82µg/mL, corresponding to 100µg/mL of DXP. A decrease of cytokines concentration was clearly observed resulting from the anti-inflammatory effect of DXP-NPs (Figure 7). The MCP-1 chemokine (Figure 7a) was strongly and significantly reduced by DXP-NPs in the presence of LPS. Regardless of DXP concentration in nanoparticles, no dose-effect was observed, meaning that the lower concentration of DXP-NPs (1µg/mL) was sufficient to yield the expected anti-inflammatory effect. The same conclusions hold for the secretion of IL-10 (Figure 7b). Indeed, a significant reduction of IL-10 level was observed after treatment with DXP nanoparticles, regardless of DXP concentrations. Concerning IL-6 release (Figure 7c), results were more balanced. No significant reduction was detected for DXP nanoparticles and free dexamethasone, but a downward trend can be observed when comparing positive control and DXP-NPs activity. This result can be related to the usual classification of IL-6 as a simultaneous pro- and anti-inflammatory cytokine. Interestingly, DXP concentration in nanoparticles has an impact on TNFα release (Figure 7d). Indeed, only 100µg/mL DXP in nanoparticles could reduce significantly the release of this important pro-inflammatory cytokine, whereas no effect was detected with free dexamethasone phosphate at the equivalent concentration.

A control study was performed to ensure that DXP-NPs do not induce inflammation by themselves (Figure S2). All these results confirmed that the use of a prodrug and its formulation into nanoparticles does not affect the therapeutic activity of the drug. DXM is most probably released

from DXP-NPs due to the presence of esterases in the cell culture medium, as it was observed in plasma [41] or even in macrophage lysosomal compartments. Based on these promising results, *in vivo* studies were performed.

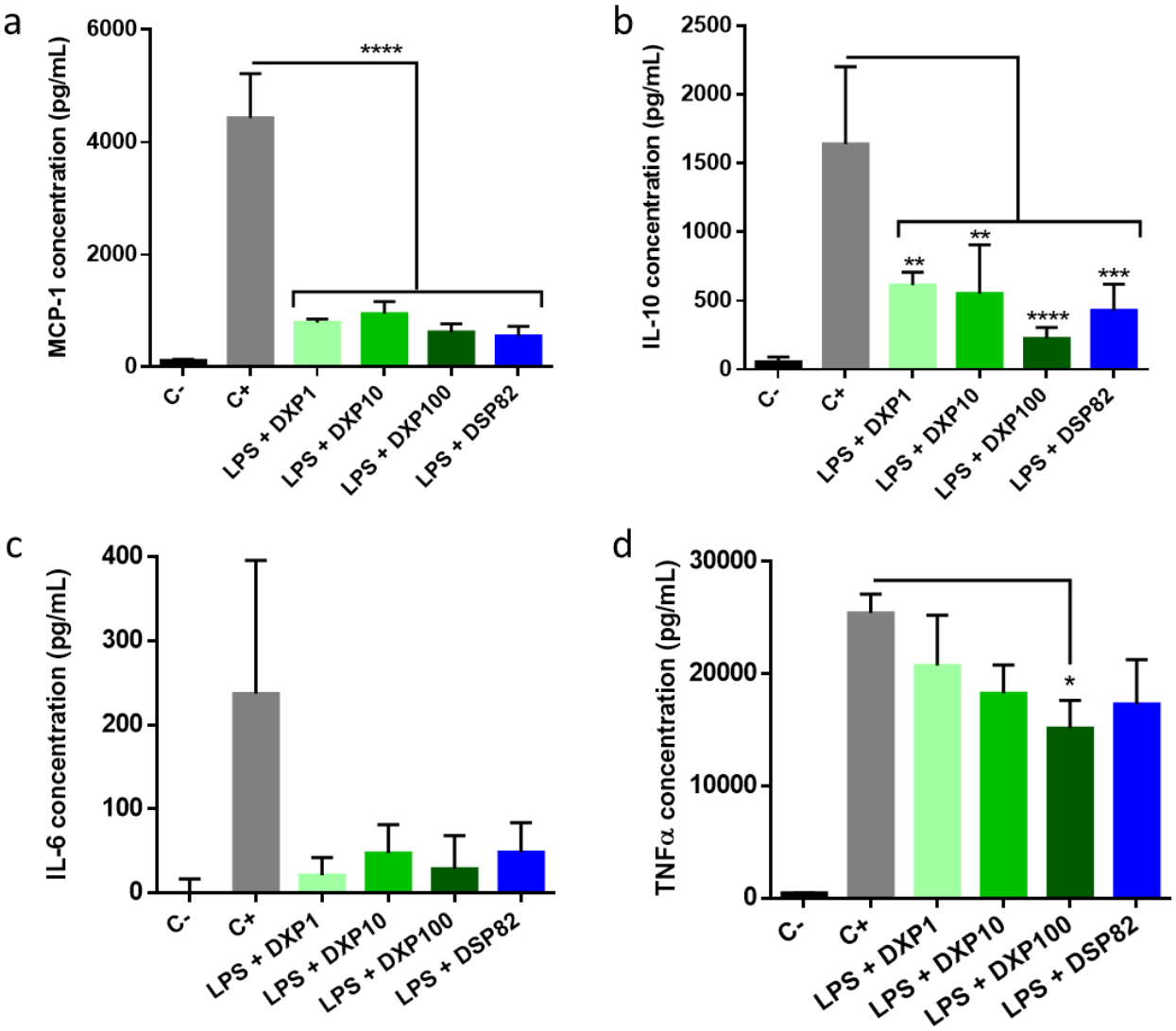

Figure 7. Cytokine production by Raw 264.7 macrophages without LPS induction (C-) or with LPS induction 0.1µg/mL (C+), DXP nanoparticles at 1µg/mL DXP (LPS+DXP1), 10µg/mL (LPS+DXP10), 100µg/mL (LPS+DXP100) or DSP solution at 82µg/mL corresponding to 100µg/mL of DXP (LPS+DSP82). Four cytokines were evaluated **a)** MCP-1, **b)** IL-10, **c)** IL-6 and **d)** TNF-α. Results are presented as mean±SEM (n=3) for all groups. Statistical analysis was performed with two-way ANOVA followed by Tukey's post test using GraphPad Prism. * $p<0.05$, ** $p<0.01$, *** $p<0.001$, **** $p<0.0001$ indicates differences with positive control (C+).

3.5 Pharmacokinetics and biodistribution

To obtain a better understanding of the behavior of DXP-NPs after IV injection, their pharmacokinetics and biodistribution were determined. Dexamethasone palmitate is a prodrug and

dexamethasone base (DXM) is the active drug released from DXP after ester bond hydrolysis. Thereby, DXM and DXP were quantified from mice plasma after DXP-NPs were intravenously injected. DXP-NPs were compared to control DSP, water-soluble prodrug of DXM (Figure 8a). Ten minutes after injection, DXM from DSP control solution was obviously eliminated very fast, reaching a plateau around 10% of the injected dose up to 48h. DXP plasmatic concentration decreases slowly until 8h after injection. After 8h, no DXP was detected in mice plasma. The prodrug is transformed into DXM, which plasmatic concentration presents a slow decrease for 18h. The main pharmacokinetic parameters were calculated according to a non-compartmental model (Figure 8b). The area under the curve ($AUC_{0-\infty}$) of DXM from nanoparticles 126400µmol*min/L, whereas DXM from control was 93600µmol*min/L meaning the active DXM molecule exposure in the body is 1.35 times higher compared to injection of free dexamethasone. When comparing data up to 4h, the $AUC_{(0-240)}$ is 3.3 fold higher for DXM from nanoparticles. At T_{max}, 10min for both, C_{max} of DXM from nanoparticles, 327µmol/L (or 128.5µg/mL) is 5.8 times higher than the control, C_{max}= 56µmol/L (or 22.1µg/mL). Volumes of distribution (Vd) reveal DXP-NPs were less distributed in the organs and stay longer in the blood, with Vd for DXM from nanoparticles 1.8-fold lower than the control. However, elimination half-life and mean residence time (MRT) are higher for the control DSP, probably due to the plasmatic plateau observed. These data support the fact that DXP-NPs lead to a higher exposure after IV injection compared to the free drug, due to the enhanced pharmacokinetics properties of DXP-NPs. Nevertheless, DXP act as a prodrug, encapsulated into NPs and seems to be rapidly hydrolyzed to release free DXM in the blood.

a

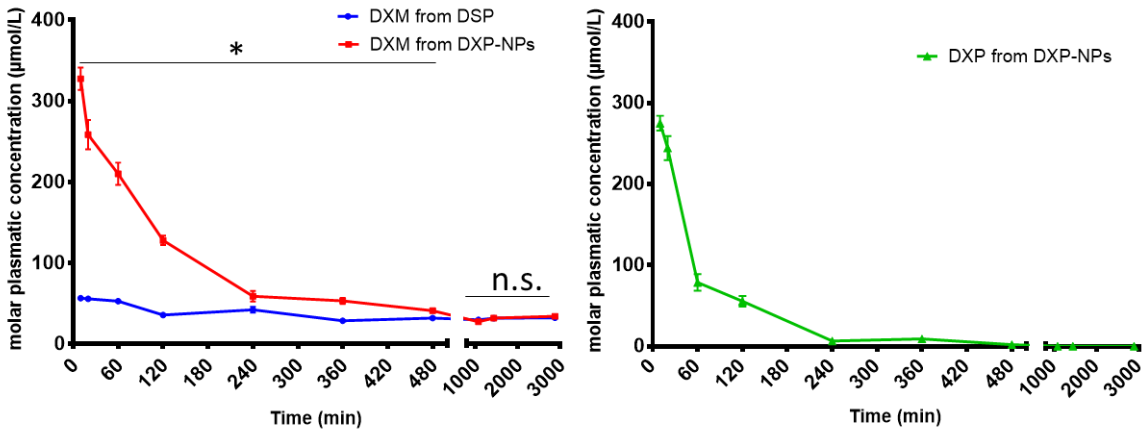

b

Pharmacokinetic parameters	DXM from DSP	DXM from DXP-NPs
$t_{1/2}$ (min)	3924	971
T_{max} (min)	10	10
C_{max} (µmol/L)	56	327
C_0 (µmol/L)	57.2	414.9
$AUC_{0-\infty}$ (µmol*min/L)	93600	126400
$AUC_{0-240min}$ (µmol*min/L)	10015	33600
MRT (min)	6115	1967
Clearance (L/min)	2.1×10^{-6}	3.3×10^{-6}
Vd (mL)	12.8	6.5

Figure 8. a. Pharmacokinetics of DXP and DXM expressed as molar plasmatic concentration. Plasma concentrations of DXP (green) and DXM (red) released from DXP nanoparticles and DXM (blue) released from DSP solution after IV injection of 12mg/kg *(eq.DXM)* on males DBA/1 healthy mice. Results are presented as mean±SEM (n=7). PK curves were significantly different up to 480min (6 hours) (* $p < 0.05$, unpaired t-test). **b.** Corresponding pharmacokinetic parameters.

Figure 9 presents the biodistribution of DXP-NPs and DSP control, both injected intravenously at 12mg/kg (*eq.DXM),* in liver, spleen, kidneys, and lungs. Among the four organs, the liver presents the highest accumulation of DXM from nanoparticles with an increase up to 18% of the injected dose 40 min after injection followed by a slow decrease until 48h. However, DXP and DXM liver concentrations from nanoparticles were clearly lower than the control DSP for the first-time points after injection. Less than 2% of the injected dose of drug or prodrug was detected in the kidneys. This presence is linked to the elimination of the molecules through urinary excretion. Very small quantities, lower than 1%, were detected in the lungs. After statistical analysis, a significant difference was found between DXM from DSP and DXM from DXP-NPs on the whole data in the spleen, whereas values in the liver, kidneys, and lungs were not significantly different (unpaired t-test). Pharmacokinetics results are correlated with biodistribution evaluation. In the liver, the small amounts of DXP detected indicate that PEGylation of nanoparticles allows a reduction of their opsonization, helping them to escape from the immune system recognition in the bloodstream. The

presence of DXM from DXP-NPs and from DSP in the liver is linked to the intrinsic hepatic accumulation of DXM.[42] On the other hand, DXP spleen concentrations from the nanoparticles were significantly higher compared to DSP. Even though DXP in spleen represents less than 2% of the injected dose, its highest concentration in this organ could be explained by the presence of the PEG at the surface of the nanoparticles. [43] Indeed, the spleen is less accessible than liver due to its low vascularization, however, the modified pharmacokinetics properties of DXP-NPs induce more accumulation in this organ compared to free drug. Very low DXP quantities were observed in the lungs proving no crystallization or aggregation of the particles occurred after IV injection. DXP-NPs stability in the blood is therefore attested.

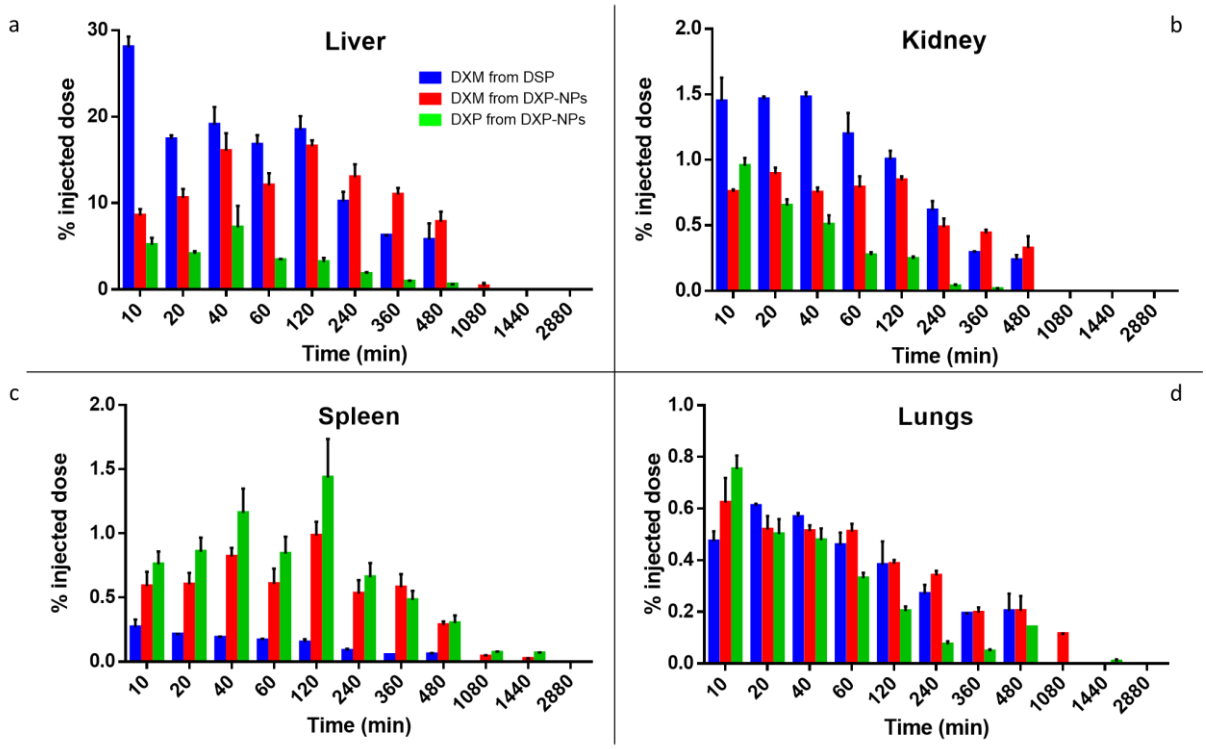

Figure 9. Biodistribution of DXP-NPs (DXP in green, DXM in red) and DSP solution (DXM in blue) after 12mg/kg *(eq.DXM)* injected dose on male DBA/1 mice. Quantification was performed in **a)** liver (not significant (n.s.) between DXM from DSP and DXM from NPs, unpaired t-test), **b)** kidney (n.s. between DXM from DSP and DXM from NPs, unpaired t-test), **c)** spleen ($p < 0.05$ between DXM from DSP and DXM from NPs, unpaired t-test) and **d)** lungs (n.s. between DXM from DSP and DXM from NPs, unpaired t-test). Results are presented as mean±SEM (n=5).

4 CONCLUSIONS

We have succeeded to formulate a hydrophobic prodrug of dexamethasone into PEGylated solid lipid nanoparticles using two different formulation processes. Either nanoprecipitation or emulsion-evaporation leads to the formation of stable nanoparticles. Nanoparticle size can be tuned between

130 and 300nm depending on the process, the prodrug/lipid ratio, and the prodrug concentration. A very high prodrug entrapment efficiency of 98% w/w was reached for both processes, corresponding to a very high equivalent DXM loading around 50% w/w. In terms of PEGylated lipid association, emulsion-evaporation method enables 53% of DSPE-PEG_{2000} entrapment whereas only 20% was obtained by nanoprecipitation. Since DXP-NPs obtained by emulsion-evaporation were smaller in size and allowed to obtain very dense PEG brushes on their surface with an available surface of 0.93nm^2/PEG chain, they were considered the perfect candidates for further *in vitro* and *in vivo* evaluation. After IV injection of DXP-NPs, the release of DXM in plasma was clearly controlled up to 18h compared to the free drug rapidly eliminated from plasma after administration. These prodrug nanoparticles represent a promising treatment for chronic inflammatory diseases as they possess all the prerequisites to accumulate in inflamed tissues after extravasation.

ACKNOWLEDGMENTS

The present work has benefited also from the core facilities of Imagerie-Gif, (http://www.i2bc.paris-saclay.fr), member of IBiSA (http://www.ibisa.net), supported by "France-BioImaging" (ANR-10-INBS-04-01), and the Labex "Saclay Plant Science" (ANR-11-IDEX-0003-02). Institut Galien Paris-Sud is a member of the Laboratory of Excellence LERMIT supported by a grant from ANR (ANR-10-LABX-33).

Authors would like to acknowledge the precious help of S. Denis for cell culture, Ivana Stolfa for HPLC-ELSD settings and quantification, Claire Gueutin for HPLC-UV and Henri Benech for pharmacokinetics analysis.

ASSOCIATED CONTENT

Supporting information

Additional figures as noted in the text: DXP crystals apparition after nanoparticles storage at room temperature during more than 37 days (S1); Cytokine production by Raw 264.7 macrophages with or without LPS induction after exposure to DXP nanoparticles (S2).

AUTHOR INFORMATION

Corresponding Author

*Phone: +33146835568. Fax: +33146835946. E-mail: elias.fattal@u-psud.fr

ORCID

Elias Fattal: 0000-0002-3194-961X

Notes

The authors declare no competing financial interest.

REFERENCES

(1) McDonough, A. K.; Curtis, J. R.; Saag, K. G. The Epidemiology of Glucocorticoid-Associated Adverse Events. *Curr. Opin. Rheumatol.* **2008**, *20* (2), 131–137.

(2) Saag, K. G.; Koehnke, R.; Caldwell, J. R.; Brasington, R.; Burmeister, L. F.; Zimmerman, B.; Kohler, J. a; Furst, D. E. Low Dose Long-Term Corticosteroid Therapy in Rheumatoid Arthritis: An Analysis of Serious Adverse Events. *Am. J. Med.* **1994**, *96* (2), 115–123.

(3) Allen, T. M. The Use of Glycolipids and Hydrophilic Polymers in Avoiding Rapid Uptake of Liposomes by the Mononuclear Phagocyte System. *Adv. Drug Deliv. Rev.* **1994**, *13* (3), 285–309. https://doi.org/10.1016/0169-409X(94)90016-7.

(4) Metselaar, J. M.; Wauben, M. H. M.; Wagenaar-Hilbers, J. P. A.; Boerman, O. C.; Storm, G. Complete Remission of Experimental Arthritis by Joint Targeting of Glucocorticoids with Long-Circulating Liposomes. *Arthritis Rheum.* **2003**, *48* (7), 2059–2066. https://doi.org/10.1002/art.11140.

(5) Gómez-Gaete, C.; Tsapis, N.; Besnard, M.; Bochot, A.; Fattal, E. Encapsulation of Dexamethasone into Biodegradable Polymeric Nanoparticles. *Int. J. Pharm.* **2007**, *331* (2), 153–159. https://doi.org/10.1016/j.ijpharm.2006.11.028.

(6) Gómez-Gaete, C.; Fattal, E.; Silva, L.; Besnard, M.; Tsapis, N. Dexamethasone Acetate Encapsulation into Trojan Particles. *J. Control. Release* **2008**, *128* (1). https://doi.org/10.1016/j.jconrel.2008.02.008.

(7) Allen, T. M.; Cullis, P. R. Liposomal Drug Delivery Systems: From Concept to Clinical Applications. *Adv. Drug Deliv. Rev.* **2013**, *65* (1), 36–48. https://doi.org/10.1016/j.addr.2012.09.037.

(8) Allen, T. M.; Cleland, L. G. Serum-Induced Leakage of Liposome Contents. *BBA - Biomembr.* **1980**, *597* (2), 418–426. https://doi.org/10.1016/0005-2736(80)90118-2.

(9) Barenholz, Y. Relevancy of Drug Loading to Liposomal Formulation Therapeutic Efficacy. *J. Liposome Res.* **2003**, *13* (1), 1–8. https://doi.org/10.1081/LPR-120017482.

(10) Teeranachaideekul, V.; Junyaprasert, V. B.; Souto, E. B.; M??ller, R. H. Development of Ascorbyl Palmitate Nanocrystals Applying the Nanosuspension Technology. *Int. J. Pharm.* **2008**, *354* (1–2), 227–234. https://doi.org/10.1016/j.ijpharm.2007.11.062.

(11) Boissenot, T.; Fattal, E.; Bordat, A.; Houvenagel, S.; Valette, J.; Chacun, H.; Gueutin, C.; Tsapis, N. Paclitaxel-Loaded PEGylated Nanocapsules of Perfluorooctyl Bromide as Theranostic Agents. *Eur. J. Pharm. Biopharm.* **2016**, *108*, 136–144. https://doi.org/10.1016/j.ejpb.2016.08.017.

(12) Scherphof, G.; Roerdink, F.; Waite, M.; Parks, J. Disintegration of Phosphatidylcholine

Liposomes in Plasma As a Result of Interaction With High-Density Lipoproteins. *Biochim. Biophys. Acta* **1978**, *542*, 296–307.

(13) Tsotas, V.-A.; Mourtas, S.; Antimisiaris, S. G. Dexamethasone Incorporating Liposomes: Effect of Lipid Composition on Drug Trapping Efficiency and Vesicle Stability. *Drug Deliv.* **2007**, *14* (7), 441–445. https://doi.org/10.1080/10717540701603530.

(14) Daull, P.; Paterson, C. a; Kuppermann, B. D.; Garrigue, J.-S. A Preliminary Evaluation of Dexamethasone Palmitate Emulsion: A Novel Intravitreal Sustained Delivery of Corticosteroid for Treatment of Macular Edema. *J. Ocul. Pharmacol. Ther.* **2013**, *29* (2), 258–269. https://doi.org/10.1089/jop.2012.0044.

(15) Wijagkanalan, W.; Higuchi, Y.; Kawakami, S.; Teshima, M.; Sasaki, H.; Hashida, M. Enhanced Anti-Inflammation of Inhaled Dexamethasone Palmitate Using Mannosylated Liposomes in an Endotoxin-Induced Lung Inflammation Model. *Mol. Pharmacol.* **2008**, *74* (5), 1183–1192. https://doi.org/10.1124/mol.108.050153.chemoattractant-1.

(16) Hong Kee, S.; Hack Joo, K.; Hyun Pyo, K.; Lee, H. J.; Si Myung, B. Liposomes with Anti-Inflammatory Steroid Prednisolone Palmitate. *Drug Dev. Ind. Pharm.* **1988**, *4* (6), 765–777.

(17) Yokoyama, K.; Watanabe, M. Limethason as a Lipid Microsphere Preparation: An Overview. *Adv. Drug Deliv. Rev.* **1996**, *20* (2–3), 195–201.

(18) Kim, J.-K.; Howard, M. D.; Dziubla, T. D.; Rinehart, J. J.; Jay, M.; Lu, X. Uniformity of Drug Payload and Its Effect on Stability of Solid Lipid Nanoparticles Containing an Ester Prodrug. *ACS Nano* **2011**, *5* (1), 209–216. https://doi.org/10.1021/nn102357y.

(19) Benameur, H.; Gand, G. De; Brasseur, R.; Vooren, J. P. Van; Legros, F. J. Liposome-Incorporated Dexamethasone Palmitate : Chemical and Physical Properties. *Int. J. Pharm.* **1993**, *89*, 157–167.

(20) Teshima, M.; Kawakami, S.; Nishida, K.; Nakamura, J.; Sakaeda, T.; Terazono, H.; Kitahara, T.; Nakashima, M.; Sasaki, H. Prednisolone Retention in Integrated Liposomes by Chemical Approach and Pharmaceutical Approach. *J. Control. Release* **2004**, *97* (2), 211–218. https://doi.org/10.1016/j.jconrel.2004.03.011.

(21) Bias, P.; Labrenz, R.; Rose, P. Sustained-Release Dexamethasone Palmitate - Pharmacokinetics and Efficacy in Patients with Activated Inflammatory Osteoarthritis of the Knee. *Clinical Drug Investigation*. 2001, pp 429–436.

(22) Mizushima, Y.; Hamano, T.; Yokoyama, K. Tissue Distribution and Anti-Inflammatory Activity of Corticosteroids Incorporated in Lipid Emulsion. *Ann. Rheum. Dis.* **1982**, *41* (3), 263–267.

(23) Gaudin, A.; Yemisci, M.; Eroglu, H.; Lepetre-Mouelhi, S.; Turkoglu, O. F.; Donmez-Demir, B.; Caban, S.; Sargon, M. F.; Garcia-Argote, S.; Pieters, G.; et al. Squalenoyl Adenosine

Nanoparticles Provide Neuroprotection after Stroke and Spinal Cord Injury. *Nat Nanotechnol* **2014**, *9* (12), 1054–1062. https://doi.org/10.1038/nnano.2014.274.

(24) Maksimenko, A.; Dosio, F.; Mougin, J.; Ferrero, A.; Wack, S.; Reddy, L. H.; Weyn, A.-A.; Lepeltier, E.; Bourgaux, C.; Stella, B.; et al. A Unique Squalenoylated and Nonpegylated Doxorubicin Nanomedicine with Systemic Long-Circulating Properties and Anticancer Activity. *Proc. Natl. Acad. Sci. U. S. A.* **2014**, *111* (2), E217-26. https://doi.org/10.1073/pnas.1313459110.

(25) Quan, L.; Zhang, Y.; Crielaard, B. J.; Dusad, A.; Lele, S. M.; Rijcken, C. J. F.; Metselaar, J. M.; Kostková, H.; Etrych, T.; Ulbrich, K.; et al. Nanomedicines for Inflammatory Arthritis: Head-to-Head Comparison of Glucocorticoid-Containing Polymers, Micelles, and Liposomes. *ACS Nano* **2014**, *8* (1), 458–466. https://doi.org/10.1021/nn4048205.

(26) Leng, D.; Chen, H.; Li, G.; Guo, M.; Zhu, Z.; Xu, L.; Wang, Y. Development and Comparison of Intramuscularly Long-Acting Paliperidone Palmitate Nanosuspensions with Different Particle Size. *Int. J. Pharm.* **2014**, *472* (1–2), 380–385. https://doi.org/10.1016/j.ijpharm.2014.05.052.

(27) Mosmann, T. Rapid Colorimetric Assay for Cellular Growth and Survival: Application to Proliferation and Cytotoxicity Assays. *J. Immunol. Methods* **1983**, *65* (1–2), 55–63. https://doi.org/10.1016/0022-1759(83)90303-4.

(28) Altman, D. G.; Festing, M. F. W. Guidelines for the Design and Statistical Analysis of Experiments Using Laboratory Animals. *ILAR J.* **2002**, *43* (4), 244–258. https://doi.org/10.1093/ilar.43.4.244.

(29) Quan, L.; Zhang, Y.; Dusad, A.; Ren, K.; Purdue, P. E.; Goldring, S. R.; Wang, D. The Evaluation of the Therapeutic Efficacy and Side Effects of a Macromolecular Dexamethasone Prodrug in the Collagen-Induced Arthritis Mouse Model. *Pharm. Res.* **2016**, *33* (1), 186–193. https://doi.org/10.1007/s11095-015-1776-1.

(30) Doi, M.; Ishida, T.; Sugio, S.; Imagawa, T.; Inoue, M. Physicochemical Properties of Dexamethasone Palmitate, a High Fatty Acid Ester of an Anti-Inflammatory Drug: Polymorphism and Crystal Structure. *J. Pharm. Sci.* **1989**, *78* (5), 417–422.

(31) Lu, X.; Howard, M. D.; Mazik, M.; Eldridge, J.; Rinehart, J. J.; Jay, M.; Leggas, M. Nanoparticles Containing Anti-Inflammatory Agents as Chemotherapy Adjuvants: Optimization and in Vitro Characterization. *AAPS J.* **2008**, *10* (1), 133–140. https://doi.org/10.1208/s12248-008-9013-z.

(32) Teeranachaideekul, V.; Müller, R. H.; Junyaprasert, V. B. Encapsulation of Ascorbyl Palmitate in Nanostructured Lipid Carriers (NLC)-Effects of Formulation Parameters on Physicochemical Stability. *Int. J. Pharm.* **2007**, *340* (1–2), 198–206. https://doi.org/10.1016/j.ijpharm.2007.03.022.

(33) Wang, R.; Xiao, R.; Zeng, Z.; Xu, L.; Wang, J. Application of Poly(Ethylene Glycol)-Distearoylphosphatidylethanolamine (PEG-DSPE) Block Copolymers and Their Derivatives as Nanomaterials in Drug Delivery. *Int. J. Nanomedicine* **2012**, *7*, 4185–4198. https://doi.org/10.2147/IJN.S34489.

(34) Vetter, T.; Mazzotti, M.; Brozio, J. Slowing the Growth Rate of Ibuprofen Crystals Using the Polymeric Additive Pluronic F127. *Cryst. Growth Des.* **2011**, *11* (9), 3813–3821. https://doi.org/10.1021/cg200352u.

(35) Warren, D. B.; Benameur, H.; Porter, C. J. H.; Pouton, C. W. Using Polymeric Precipitation Inhibitors to Improve the Absorption of Poorly Water-Soluble Drugs : A Mechanistic Basis for Utility. *J. Drug Target.* **2010**, *18* (August), 704–731. https://doi.org/10.3109/1061186X.2010.525652.

(36) Yuan, F.; Dellian, M.; Fukumura, D.; Leunig, M.; Berk, D. A.; Torchilin, V. P.; Jain, R. K. Vascular Permeability in a Human Tumor Xenograft : Molecular Size Dependence and Cutoff Size Advances in Brief Vascular Permeability in a Human Tumor Xenograft : Molecular Size Dependence and Cutoff Size1. *Cancer Res.* **1995**, *55*, 3752–3756.

(37) Li, X. Size and Shape Effects on Receptor-Mediated Endocytosis of Nanoparticles. *J. Appl. Phys.* **2012**, *111* (2), 024702. https://doi.org/10.1063/1.3676448.

(38) Verma, A.; Stellacci, F. Effect of Surface Properties on Nanoparticle-Cell Interactions. *Small* **2010**, *6* (1), 12–21. https://doi.org/10.1002/smll.200901158.

(39) Ahsan, F.; Rivas, I. P.; Khan, M. A.; Suarez, A. I. T. Targeting to Macrophages : Role of Physicochemical Properties of Particulate Carriers — Liposomes and Microspheres — on the Phagocytosis by Macrophages. *J. Control. Release* **2002**, *79*, 29–40.

(40) ISO. *ISO 10993-5:2009(E) Biological Evaluation of Medical Devices- Part 5: Tests for in Vitro Cytotoxicity*; 2009.

(41) Lorscheider, M.; Tsapis, N.; Mujeeb-ur-Rehman; Gaudin, F.; Stolfa, I.; Abreu, S.; Mura, S.; Chaminade, P.; Espeli, M.; Fattal, E. Dexamethasone Palmitate Nanoparticles: An Efficient Treatment for Rheumatoid Arthritis. *J. Control. Release* **2019**, *296* (January), 179–189. https://doi.org/10.1016/J.JCONREL.2019.01.015.

(42) Begg, E. J.; Atkinson, H. C.; Gianarakis, N. The Pharmacokinetics of Corticosteroid Agents. *Med. J. Aust.* **1987**, *146* (1), 37–41. https://doi.org/10.5694/j.1326-5377.1987.tb120124.x.

(43) Peracchia, M. T.; Fattal, E.; Desmaële, D.; Besnard, M.; Noël, J. P.; Gomis, J. M.; Appel, M.; D'Angelo, J.; Couvreur, P. Stealth(®) PEGylated Polycyanoacrylate Nanoparticles for Intravenous Administration and Splenic Targeting. *J. Control. Release* **1999**, *60* (1), 121–128. https://doi.org/10.1016/S0168-3659(99)00063-2.